Suppression Control of Radial Force Vibration due to Fundamental Permanent-Magnet Flux in IPMSM

Masato Kanematsu, Takayuki Miyajima
Hiroshi Fujimoto, and Yoichi Hori
The University of Tokyo
5-1-5 Kashiwanoha,
Kashiwa, Chiba, 277-8561 Japan
kanematsu, miya@hflab.k.u-tokyo.ac.jp
fujimoto, hori@k.u-tokyo.ac.jp

Toshio Enomoto, Masahiko Kondou, Hiroshi Komiya
Kantaro Yoshimoto, and Takayuki Miyakawa
Nissan Motor Co., Ltd.
1-1, Morinosatoaoyama, Atsugi-shi
Kanagawa, 243-0123, Japan
enomoto, m-kondo, h-komiya@mail.nissan.co.jp
ka-yoshimoto, takayuki_miyakawa@mail.nissan.co.jp

***Abstract*— The relationship between electrical 2nd order radial force and dq-axis current is examined and 2nd order acceleration is suppressed in this paper. On no-load condition, flux distribution is approximated in order to calculate radial force. Radial force on a tooth is obtained by using maxwell stress equation and approximation of flux distriution. Considering cyclic nature of 3-phase, optimal d-axis current to suppress 2nd radial force which is caused by fundamental permanent flux is proposed. Simulations and experiments under load and no-load conditions are performed to show the validation of proposed optimal d-axis current reference.**

I. INTRODUCTION

IPMSMs (Interior Permanent Magnet Synchronous Motors) are widely applied in many industrial applications. In these applications, it is essential to reduce noise and vibration. Compared with other types of electrical machines such as induction motors and switched reluctance motors, IPMSMs are relatively quiet. However, in applications, such as industrial servos, consumer products, and automotive drives, low acoustic noise and vibration are demanded.

The magnetic attractive force which causes noise and vibration has both the tangential and radial components. The fluctuation of tangential magnetic force is known as torque ripple. Torque ripple triggers torsional resonant vibration and deteriorates control performance. On the other hand, radial force induces elastic deformation when the frequency of radial force corresponds to natural frequency of the stator. Each magnetic attractive force can be suppressed by current control technology and structural designing. Until now, vibration reduction is mainly achieved by the structural designing based on Finite Element Analysis (FEA).

The causes of noise and vibration in PMSMs are investigated in [1]. In [2], the relationship between skew and radial force vibration is examined. In [3], [4] and [5], vibration caused by radial force is examined with structural analysis. In [6], with FEA and experiments, a detailed study of the vibration is performed. Some papers such as References [7][8][9] propose radial force reduction using structural changes. On the other hand, few methods to suppress vibration using current control is proposed. Reference [10] proposes radial force reduction with current control in condition of no-tooth effect. However, this method is not versatile because it does not consider tooth effect and the relationship between current reference and radial force is obscure. Therefore, simpler methods which predict and reduce amplitude of radial force is required.

Radial force which is caused by permanent magnet is mainly electrical 2nd order. Considering the phase difference of U, V, and W-phase radial forces, it is known that 2nd order radial force has spatially Pth circular mode, in this sentence P denotes pole pairs. In this paper, radial force on a tooth considering magnetic flux distribution is studied firstly in case of no-load condition. The flux distribution is approximated as a series of rectangle. With this approximation, the radial force on a tooth is calculated. Considering cyclic nature of 3-phase, optimal d-axis current is derived. Secondly, q-axis influence is taken into account in magnetic field analysis by FEA. Finally, simulations and experiments under load and no-load conditions are performed to show the relationship between radial force and d-axis current.

II. MODEL AND MAXWELL STRESS

A. dq Model of IPMSM

The voltage equation of IPMSM in dq axis and the motor torque T are reporesented by

$$\begin{bmatrix} v_d \\ v_q \end{bmatrix} = \begin{bmatrix} L_d s + R & -\omega_e L_q \\ \omega_e L_d & L_q s + R \end{bmatrix} \begin{bmatrix} i_d \\ i_q \end{bmatrix} + \omega_e \Psi_a \begin{bmatrix} 0 \\ 1 \end{bmatrix}, \quad (1)$$

$$T = K_{mt} i_q + K_{rt} i_d i_q, \quad (2)$$

$$\omega_m = \frac{1}{Js + D} T, \quad (3)$$

$$\omega_e = P \omega_m, \quad (4)$$

where $v_{d,\ q}$ are the d-axis and q-axis voltage, $i_{d,\ q}$ are the d-axis and q-axis current, $L_{d,\ q}$ are the d-axis and q-axis inductance, R is the stator winding resistance, ω_e is the electric angular velocity, Ψ_a is the back EMF constant, $K_{mt} := P\Psi_a$, $K_{rt} := P(L_d - L_q)$, P is the number of pole pairs, and J is the rotor innertia. In thes paper, 2-phse/3-phase transform is represented as absolute transformation.

B. The Electromagnetic Forces of IPMSM

φ_m refers to the stator position angle between the center of a U-phase tooth and a point where maxwell stress is considered. The radial and tangential maxwell stress $f_r(\varphi_m), f_\theta(\varphi_m)$ are expressed as

$$f_r(\varphi_m) = \frac{B_r^2(\varphi_m) - B_\theta^2(\varphi_m)}{2\mu_0}, \tag{5}$$

$$f_\theta(\varphi_m) = \frac{B_r(\varphi_m)B_\theta(\varphi_m)}{\mu_0}, \tag{6}$$

where $B_r(\varphi_m)$ and $B_\theta(\varphi_m)$ are the radial and tangential flux densities on φ_m. In this paper, radial forces $F_{rU,rV,rW}$ on the surfaces of U, V and W-phase teeth are evaluated as

$$F_{rU,rV,rW} = \int\int f_r(\varphi_m)\mathrm{d}S, \tag{7}$$

where S is the surface area on a tooth facing on the air gap.

III. APPROXIMATE MODEL OF FLUX DISTRIBUTION

In this paper, radial force is calculated using approximate flux distribution. In this section, approximate radial flux distribution is derived. JMAG (electromagnetic field analysis software) produced by JSOL Corporation is utilized for this analysis.

A. Hypotheses of Approximation

The value of $B_r(\varphi_m)$ is decided by i_d, i_q, φ_m, and the rotor angle θ_e. Here, it is assumed that the magnetic flux of permanent magnet $B_r(\varphi_m)$ is expressed as

$$B_r(\varphi_m) = B_{ri_d}(\varphi_m, i_d) + B_{ri_q}(\varphi_m, i_q) + B_{rm}(\varphi_m), \tag{8}$$

where $B_{ri_d}(\varphi_m, i_d)$, $B_{ri_q}(\varphi_m, i_d)$ are the radial flux densities due to i_d and i_q on φ_m, and $B_{rm}(\varphi_m)$ is radial flux density which is attributable to Ψ_a on φ_m. Firstly, in order to consider no-load condition, $B_{ri_q}(\varphi_m, i_q)$ is neglected, and $B_{ri}(\varphi_m, i_d)$ denotes $B_{ri_d}(\varphi_m, i_d)$ in this paper.

In this paper, the linearity between i_d and $B_{ri_d}(\varphi_m)$ is assumed. Generally, $B_\theta^2(\varphi_m)$ is much smaller than $B_r^2(\varphi_m)$ and (5) can be approximated as

$$f_r(\varphi_m) \approx \frac{B_r^2(\varphi_m)}{2\mu_0}. \tag{9}$$

B. Approximate Model of Flux Distribution by Permanent Magnet

FEA result of flux distribution by permanent magnet is shown in Fig. 1. As shown in Fig. 1, The flux distribution is nearly flat on U-phase teeth but unequal on V and W-phase teeth. Here, the flux distribution is approximated by rectangle. The magnetic flux passes through the area γS and no magnetic flux passes through the other area γS. $\gamma(0 < \gamma \leq 1)$ is flux interlinkage area. It is expected that γ depends on rotor structure but this relationship is inevident. In this paper, γ is determined from FEA such that $\gamma = 1$ on U-phase and $\gamma = 0.5$ on V and W-phases.

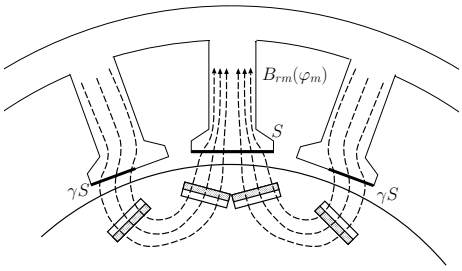

(a) magnetic flux lines

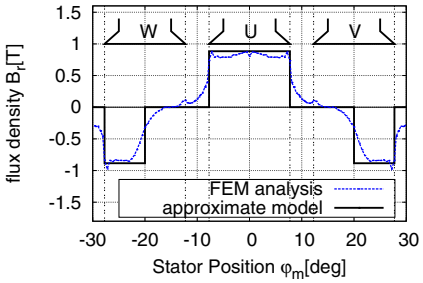

(b) $B_{rm}(\varphi_m)$

Fig. 1. flux distribution $B_{rm}(\varphi_m)$ by permanent magnet

The interlinkage flux $\phi_{mU,mV,mW}$ on a tooth surface is calculated as

$$\phi_{mU} = \phi, \quad \phi_{mV,mW} = -\frac{1}{2}\phi, \tag{10}$$

where N is the number of turn/teeth, $\phi := \sqrt{\frac{2}{3}}\frac{\Psi_a}{PN}$. Here, $\sqrt{\frac{2}{3}}$ is the coefficient to transform two-phase into three-phase.

The flux distribution of permanent magnet is approximated as $B_{rmj} = \frac{\phi_{mj}}{S_j}$, where B_{rmj} is the flux interlinkage of j-phase teeth by permannet magnet, ϕ_{mj} is interlinkage flux of j-phase, S_j is interlinkage flux area on j-phase teeth. Fig. 1 shows the approximate model of flux distribution.

C. Approximate Model of Flux Distribution by d-axis Current

Based on linear independency, $B_{ri_d}(\varphi_m)$ is calculated by the diffenrence between B_r as $i_d = -1$A and by $B_{rm}(\varphi_m)$. Fig. 2 shows the flux distribution of $B_{ri_d}(\varphi_m)$. The flux distribution on U-phase tooth is nearly flat. On the other hand, the flux distributions on V and W-phase teeth is deflected to the side of a U-phase tooth. In this paper, in order to construct a simple model, flux distributions on V and W-phase teeth are assumed to be flat.

$$\phi_{iU} = l_d i_d, \quad \phi_{iV,iW} = -\frac{1}{2}l_d i_d, \tag{11}$$

where $\varphi_{iU,iV,iW}$ are the flux on U, V and W-phase teeth by d-axis current. Here, l_d:=$\sqrt{\frac{2}{3}}\frac{L_d}{PN}$.

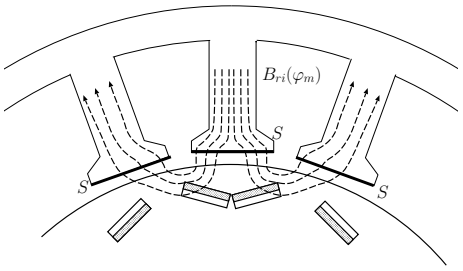

(a) magnetic flux lines

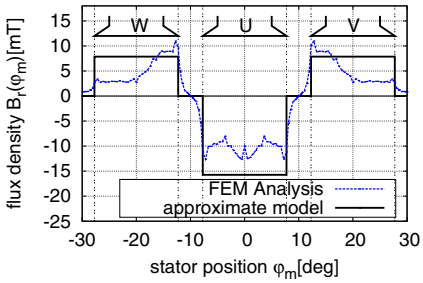

(b) $B_{ri}(\varphi_m)$

Fig. 2. flux distribution $B_{ri}(\varphi_m)$ by d-axis current

TABLE I
IPMSM PARAMETER

Stator Configuration	Concentrated winding
interlinkage area coefficient γ	0.5
d-axis 1-teeth inductance l_d	53.1 [μH]
turn number N	20
teeth area S	4.13×10^{-4} [m^2]
1-teeth magnetic flux ϕ	3.65 [mWb]

IV. RADIAL FORCE APPROXIMATION USING FLUX DISTRIBUTION

A. Radial Force on U-phase Teeth

The flux distribution $B_r(\varphi_m)$ on U-phase teeth are calculated as follows:

$$B_r(\varphi_m) = \left(\frac{\phi}{S} + \frac{l_d i_d}{S}\right). \tag{12}$$

By substituting (5) and (12) into (7), (14) is obtaind.

$$F_{rU} = \frac{B_r^2(\varphi_m)}{2\mu_0} \cdot S \tag{13}$$

$$= \frac{(\phi + l_d i_d)^2}{2\mu_0 S} \tag{14}$$

B. Radial Force on V and W-phase Teeth

The flux distribution by permanent magnet is not flat on V and W-phase teeth. Therefore, approximate radial force is derived in two areas. Fig. 3(b) shows flux distibution image on V and W-phase. In Fig. 3(b), the flux distribution $B_r(\varphi_m)$, $B'_r(\varphi_m)$ is calculated as follows:

$$B_r(\varphi_m) = \left(\frac{\phi}{2\gamma S} + \frac{l_d i_d}{2S}\right) \tag{15}$$

$$B'_r(\varphi_m) = \frac{l_d i_d}{2S} \tag{16}$$

The radial forces F_{rV}, F_{rW} on V, and W-phase teeth are obtained as

$$F_{rV}, F_{rW} = \frac{{B_r}^2(\varphi_m)}{2\mu_0} \cdot \gamma S + \frac{{B'_r}^2(\varphi_m)}{2\mu_0} \cdot (1-\gamma) S \tag{17}$$

$$= \frac{(\phi + l_d i_d)^2 + \frac{(1-\gamma)}{\gamma}\phi^2}{8\mu_0 S}. \tag{18}$$

C. Derivation of Current Reference to Suppress 2nd Order Radial Force

In this section, d-axis current reference is derived to suppress 2nd order radial force. $F_{rU}(\theta_e), F_{rV}(\theta_e)$, and $F_{rW}(\theta_e)$ refer to radial forces of U, V and W-phase teeth when rotor electrical angle is θ_e.

Generally, it is preferred that the 2nd order radial force amplitude is zero. When θ_e is 0 or π rad, the radial force on U-phase teeth is maximum and equals $F_{rU}(0)$ which is obtained in (14). Radial force reaches the a minimum value when θ_e is $\frac{1}{2}\pi$ or $\frac{3}{2}\pi$ rad. But, at these points, approximation model is not accurate enough. Therefore, radial force at $\theta_e = \frac{1}{3}\pi$ rad is used instead of $\theta_e = \frac{1}{2}\pi$ rad. If three-phase equilibrium is assumed, $F_{rU}(\frac{2}{3}\pi)$ equals $F_{rV}(0)$. $F_{rV}(0)$ is approximated in (18). Moreover, by cyclic nature, $F_{rU}(\theta_e)$ is the same values at electrical angle $\theta_e = \frac{1}{3}\pi, \frac{2}{3}\pi, \frac{4}{3}\pi$, and $\frac{5}{3}\pi$ rad. If following equation is true, it is predicted that 2nd radial force is suppressed largely.

$$F_{rU}(0) = F_{rU}\left(\frac{2}{3}\pi\right). \tag{19}$$

From (13), (17), and (18), the d-axis current which achieves minimum 2nd order radial vibration is represented by

$$i_d = \left(-1 \pm \sqrt{\frac{1-\gamma}{3\gamma}}\right)\frac{\phi}{l_d}. \tag{20}$$

By taking into consideration of $0 < \gamma \leq 1$, the i_d is real number. Here, in order to use minimum current amplitude plus sign in (20) is selected. Using Table. 1, d-axis current reference is calculated by

$$i_d = -29.1\text{A} \tag{21}$$

Simulation results is shown in Fig. 5. When $i_d = -29.1$ A, 2nd order radial force is largely suppressed. Fig. 5 shows (20) is optimal reference to suppress radial force vibration. Each tooth radial force vibrations are suppressed by over 95 % in no-load condition, by over 60 % in load condition.

D. Consideration of Flux Distribution by q-axis Current

In this chapter, the influence of flux distribution attributed by q-axis current is considered. FEA result of flux distribution of q-axis current is shown in Fig. 4. Fig. 4 shows

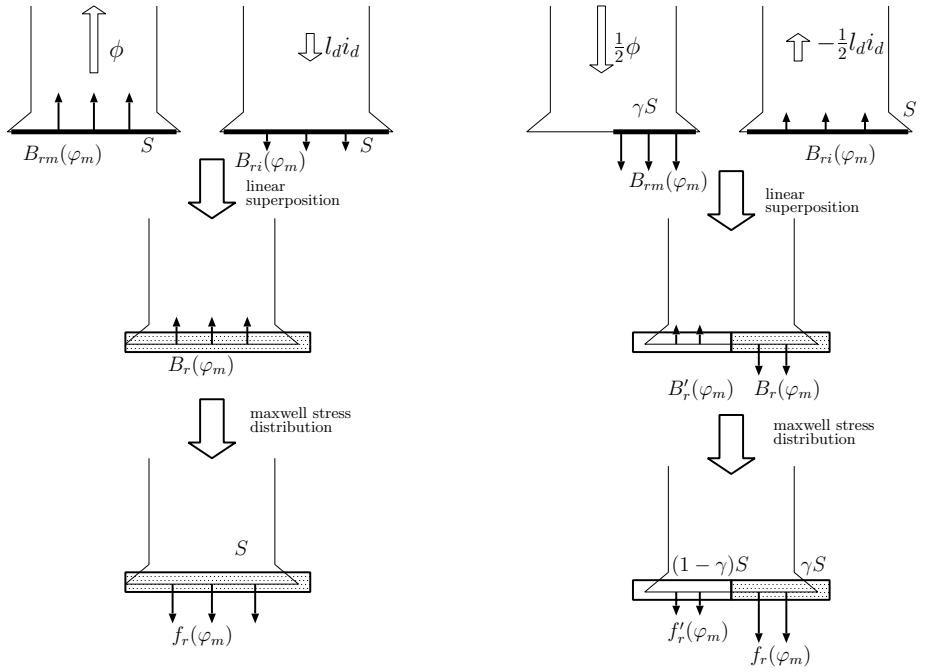

(a) flux distribution image on U-phase

(b) flux distribution image on V and W-phase

Fig. 3. radial force calculation

that flux distribution on U-phase tooth is 0. The dq/3-phase transform matrix $\boldsymbol{C}_{UVW}^{dq}$ at $\theta_e = 0$ is given by

$$\boldsymbol{C}_{UVW}^{dq} = \sqrt{\frac{2}{3}} \begin{bmatrix} 1 & 0 \\ -\frac{1}{2} & \frac{\sqrt{3}}{2} \\ -\frac{1}{2} & -\frac{\sqrt{3}}{2} \end{bmatrix}. \tag{22}$$

This means the flux by q-axis current pass only through V and W-phase teeth. In Fig. 4, magnetic flux and q-axis flux affect each other, and this leads to asymmetry of flux distribution on V and W-phase teeth.

V. EXPERIMENT

It is difficult to measure radial force directly. In this paper, radial acceleration outside the stator is evaluated in stead of radial force. Experimental environment is shown in Fig. 6. The velocity is controlled by load motor. Drive motor controls current and radial acceleration on the stator of the drive motor is measured by accelerator.

In this paper, the negative d-axis current reference is limited within -20 A because of the motor rating. Experimental results of run-up spectrograms with and without i_d current are shown in Fig. 7. The number of pole pairs are 6 in this motor, so the frequency of 2nd order acceleration is $\frac{n}{5}$[Hz], in which n is rotation speed. Fig. 7 shows 2nd and 6th acceleration is relatively larger compared with other components. 2nd acceleration increases when the frequency of 2nd radial force corresponds to the frequency of mechanical resonance. In Fig. 7, longitudinal lines, such as 400, 800, and 1600 Hz, denote mechanical resonances. Experimental results with $n = 1000$, 2000 rpm are shown in Fig. 8(a), and 8(b) respectively. Here, the frequency of x-axis is normalized by electrical angle frequency. Fig. 8(a), and 8(b) shows d-axis current suppress 2nd order acceleration effectively, but deteriorate 6th order acceleration. 2nd order spectrums extracted in Fig. 7 are shown in Fig. 8(c). 2nd order acceleration is suppressed at all rotation speeds.

VI. CONCLUSION

In this paper, optimal d-axis current reference which reduces 2nd radial force is proposed. The approximation of radial force distribution enables to calculate radial forces on teeth. The relationship between d-axis current and 2nd radial force is examined. The approximate model of 2nd radial force predict and control the amplitude of 2nd radial acceleration. Experiments were performed to show the validation of this modeling. It is shown that this method is effective at any rotation speeds.

The amplitude of high order radial force is smaller than of 2nd radial force. However, high order radial force, specially 6th order, can easily transmit stator and generate large acceleration when rotating speed equals stator natural frequency. The shape of 6th order radial force is 0th circular mode. In our future works, high order radial force modeling and control method will be realized.

REFERENCES

[1] Gieras, J.F.; Chong Wang; Joseph, C.S.L.; Ertugrul, N.; , "Analytical Prediction of Noise of Magnetic Origin Produced by Permanent Magnet Brushless Motors," Electric Machines Drives Conference, 2007. IEMDC '07. IEEE International , vol.1, no., pp.148-152, 3-5 May 2007

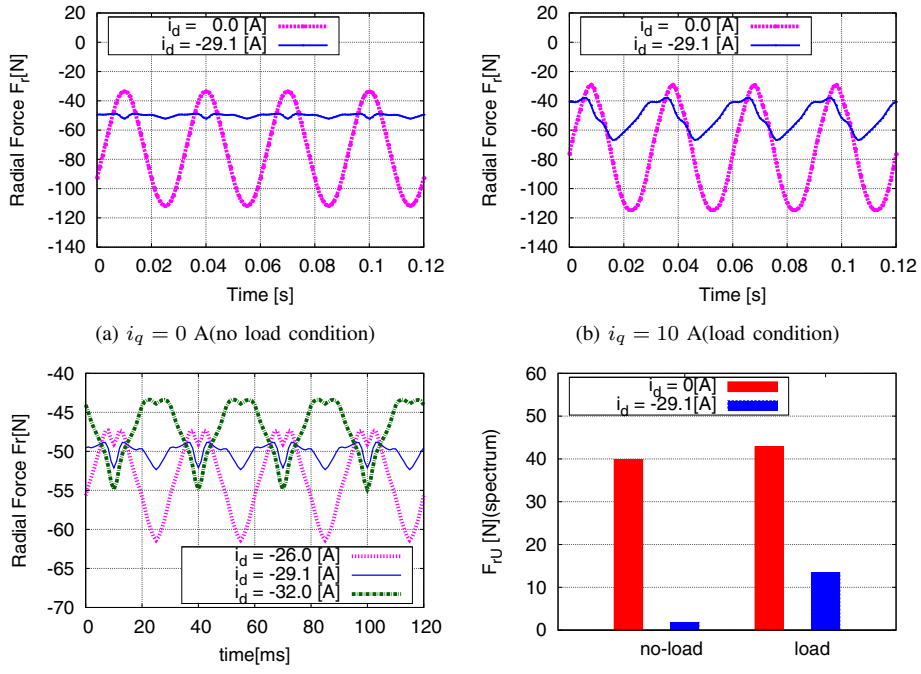

(a) $i_q = 0$ A(no load condition)

(b) $i_q = 10$ A(load condition)

(c) $i_q = 0$ A(detail)

(d) 2nd order spectrum of radial force

Fig. 5. U-phase radial force F_{rU} suppression with d-axis current

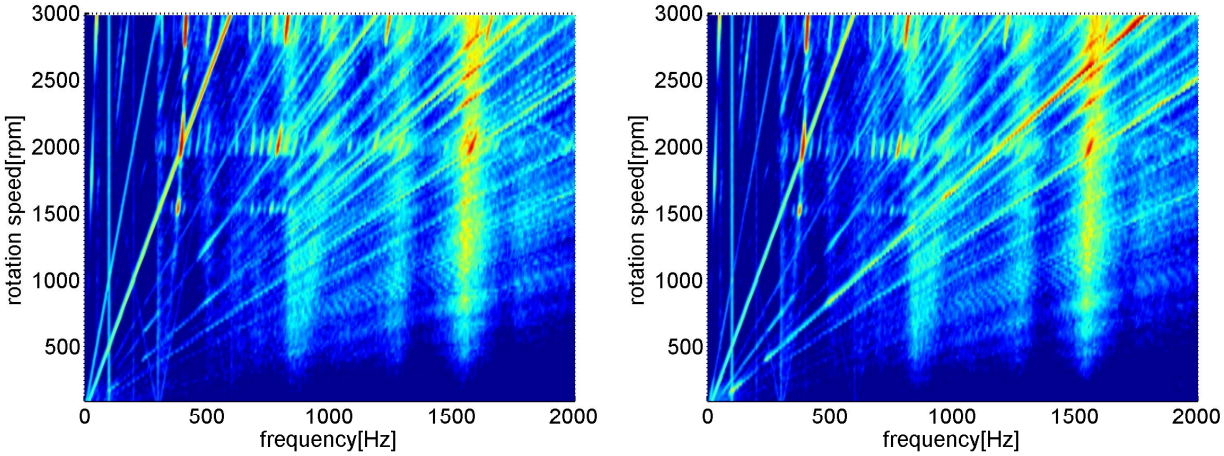

(a) i_q = 10A, i_d = 0A

(b) i_q = 10A, i_d = -20A

Fig. 7. run-up stectrograms(Experimental Result)

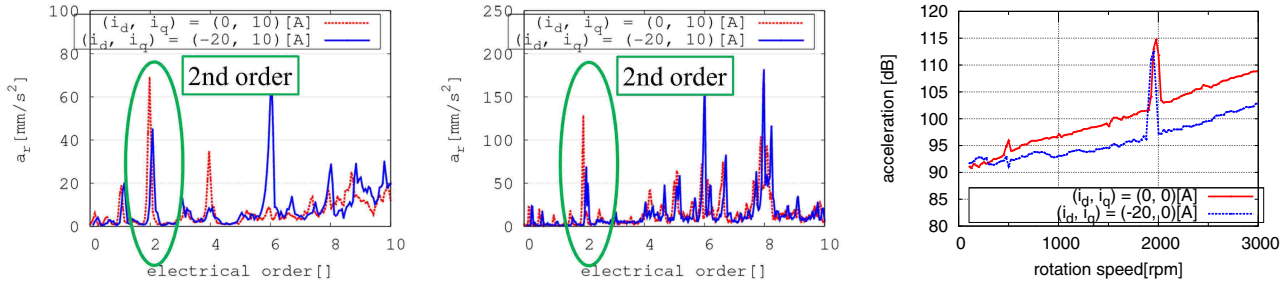

(a) 1000rpm

(b) 2000rpm

(c) comparison of 2nd order acceleration

Fig. 8. Experimental results

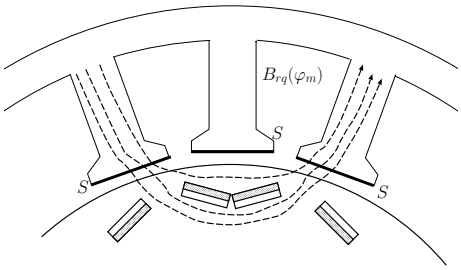

(a) magnetic flux lines

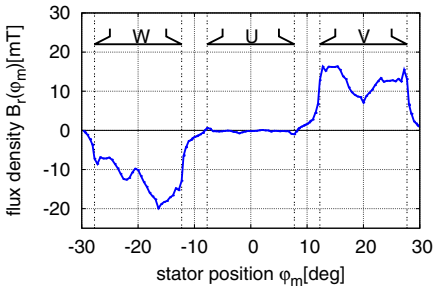

(b) $B_{ri_q}(\varphi_m)$

Fig. 4. flux distribution $B_{ri_q}(\varphi_m)$ by q-axis current

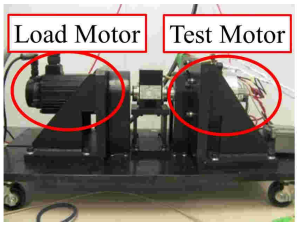

(a) motor bench

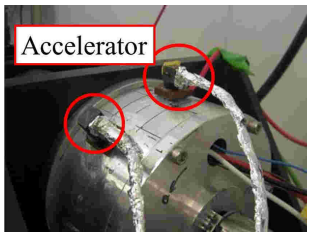

(b) accelerator

Fig. 6. Experimental Environment

[2] Jae-Woo Jung; Do-Jin Kim; Jung-Pyo Hong; Geun-Ho Lee; Seong-Min Jeon; , "Experimental Verification and Effects of Step Skewed Rotor Type IPMSM on Vibration and Noise," Magnetics, IEEE Transactions on , vol.47, no.10, pp.3661-3664, Oct. 2011

[3] Wang, J.; Xia, Z.P.; Long, S.A.; Howe, D.; , "Radial force density and vibration characteristics of modular permanent magnet brushless ac machine," Electric Power Applications, IEE Proceedings - , vol.153, no.6, pp.793-801, November 2006

[4] Islam, R.; Husain, I.; , "Analytical model for predicting noise and vibration in permanent magnet synchronous motors," Energy Conversion Congress and Exposition, 2009. ECCE 2009. IEEE , vol., no., pp.3461-3468, 20-24 Sept. 2009

[5] Islam, M.; Islam, R.; Sebastian, T.; , "Noise and vibration characteristics of permanent magnet synchronous motors using electromagnetic and structural analyses," Energy Conversion Congress and Exposition (ECCE), 2011 IEEE , vol., no., pp.3399-3405, 17-22 Sept. 2011

[6] Boesing, M.; De Doncker, R.W.; , "Exploring a vibration synthesis process for the acoustic characterization of electric drives," Electrical Machines (ICEM), 2010 XIX International Conference on , vol., no., pp.1-6, 6-8 Sept. 2010

[7] Tao Sun; Ji-Min Kim; Geun-Ho Lee; Jung-Pyo Hong; Myung-Ryul Choi; , "Effect of Pole and Slot Combination on Noise and Vibration in Permanent Magnet Synchronous Motor," Magnetics, IEEE Transactions on , vol.47, no.5, pp.1038-1041, May 2011

[8] Zhu, Z.Q.; Xia, Z.P.; Wu, L.J.; Jewell, G.W.; , "Analytical modelling and finite element computation of radial vibration force in fractional-slot permanent magnet brushless machines," Electric Machines and Drives Conference, 2009. IEMDC '09. IEEE International , vol., no., pp.144-151, 3-6 May 2009

[9] Jin Hur; Jin-Wook Reu; Byeong-Woo Kim; Gyu-Hong Kang, "Vibration Reduction of IPM-Type BLDC Motor Using Negative Third Harmonic Elimination Method of Air-Gap Flux Density," Industry Applications, IEEE Transactions on , vol.47, no.3, pp.1300,1309, May-June 2011

[10] Guandong Jiao; Rahn, C.D.; , "Field weakening for radial force reduction in brushless permanent-magnet DC motors," Magnetics, IEEE Transactions on , vol.40, no.5, pp. 3286- 3292, Sept. 2004